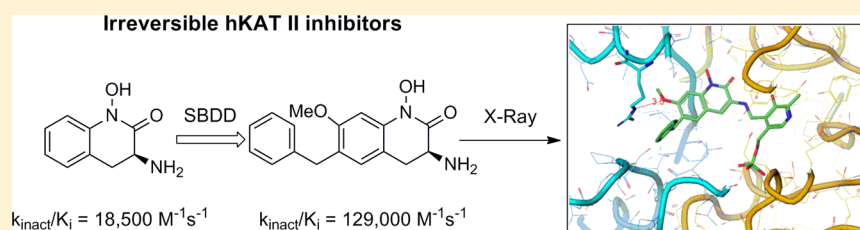


Structure-Based Design of Irreversible Human KAT II Inhibitors: Discovery of New Potency-Enhancing Interactions

Jamison B. Tuttle,^{*,†} Marie Anderson, Bruce M. Bechle, Brian M. Campbell, Cheng Chang, Amy B. Dounay, Edelweiss Evrard, Kari R. Fonseca, Xinmin Gan, Somraj Ghosh, Weldon Horner, Larry C. James, Ji-Young Kim, Laura A. McAllister, Jayvardhan Pandit, Vinod D. Parikh, Brian J. Rago, Michelle A. Salafia, Christine A. Strick, Laura E. Zawadzke, and Patrick R. Verhoest

Pfizer Worldwide Research and Development, Neuroscience Medicinal Chemistry, Eastern Point Road, Groton, Connecticut 06340, United States

Supporting Information



ABSTRACT: A series of aryl hydroxamates recently have been disclosed as irreversible inhibitors of kynurenine amino transferase II (KAT II), an enzyme that may play a role in schizophrenia and other psychiatric and neurological disorders. The utilization of structure–activity relationships (SAR) in conjunction with X-ray crystallography led to the discovery of hydroxamate **4**, a disubstituted analogue that has a significant potency enhancement due to a novel interaction with KAT II. The use of k_{inact}/K_i to assess potency was critical for understanding the SAR in this series and for identifying compounds with improved pharmacodynamic profiles.

KEYWORDS: kynurenine amino transferase, kynurenic acid, aryl hydrocarbon receptor, irreversible inhibition, hydroxamic acid, dose response modeling, *in vivo* microdialysis, schizophrenia

The kynurenine amino transferase (KAT) class of pyridoxal phosphate (PLP)-dependent transaminases catalyzes the cyclization of L-kynurenine to kynurenic acid (KYNA) in the L-tryptophan metabolic pathway.^{1,2} Recently, KYNA has been shown to agonize the arylhydrocarbon receptor (AHR), a nuclear protein involved in gene transcription and other cellular regulatory functions.³ Additionally, a burgeoning body of research implicates KYNA in a range of neurological disorders due to its antagonism of the $\alpha 7$ nicotinic acetylcholine receptor and the N-methyl-D-aspartate (NMDA) receptor.^{4,5} Elevated levels of KYNA have been found in the cerebral spinal fluid (CSF) and postmortem brain tissue of schizophrenics.^{6–8} Furthermore, individuals with bipolar disorder have also been found to have increased levels of KYNA in the CSF.⁹ Decreasing central KYNA levels in afflicted individuals may therefore provide therapeutic benefit for treating these and other psychiatric and neurological disorders.^{10,11}

Among the four homologous members of the KAT family, KAT II is largely responsible for centrally produced KYNA, thereby emerging as an attractive target for medicinal chemists.¹² As such, recent articles have reported both reversible and irreversible KAT II inhibitors.^{13–16} One useful scaffold is hydroxamate **1**, a centrally active and irreversible inhibitor of KAT II.^{14,17} Preliminary structure–activity relation-

ship (SAR) indicated that substituents were better tolerated on C6 and C7, whereas potency losses were observed with substitution on C5 and C8 (Figure 1). This SAR was supported

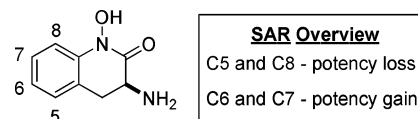


Figure 1. SAR trends on the aryl hydroxamate scaffold.

by the crystal structure, which showed that positions 6 and 7 are oriented toward a solvent-exposed region in the enzyme.¹⁴ In contrast, positions 5 and 8 are directed toward the walls of the binding pocket. As a consequence of these findings, a broad range of analogues were designed to assess the SAR of this series.^{14,15} This communication focuses on key analogues that led to the discovery of substantial potency-enhancing interactions with human KAT II.

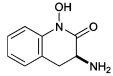
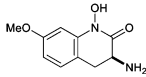
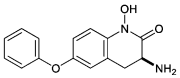
Received: August 11, 2012

Accepted: October 24, 2012

Published: October 24, 2012

At the outset, a reliable method for assessing potency of irreversible inhibition was required. For example, analysis of IC_{50} values does not discriminate potency differences among these KAT II inhibitors (Tables 1 and 2, entries 1–4), and

Table 1. Key SAR of Hydroxamate Derivatives

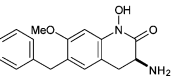
| Compound | Structure | IC_{50} (nM) | k_{inact} (min^{-1}) ^a | K_i (μM) ^b | human k_{inact}/K_i ($\text{M}^{-1}\text{s}^{-1}$) ^c |
|----------|---|----------------|--|--------------------------------------|---|
| 1 |  | 23 | 0.0156 | 0.0142 | 18,500 |
| 2 |  | 22 | 0.0137 | 0.0077 | 31,700 |
| 3 |  | 23 | 0.0108 | 0.0071 | 26,800 |

^aValues represent the geometric mean of at least three experiments.

^bValues represent the arithmetic mean of at least three experiments.

^cAdditional statistical details are provided in the Supporting Information.

Table 2. Activity of Compound 4

| Compound | Structure | IC_{50} (nM) | k_{inact} (min^{-1}) ^a | K_i (μM) ^b | human k_{inact}/K_i ($\text{M}^{-1}\text{s}^{-1}$) ^c |
|----------|--|----------------|--|--------------------------------------|---|
| 4 |  | 37 | 0.0146 | 0.0016 | 129,000 |

^aValues represent the geometric mean of at least three experiments.

^bValues represent the arithmetic mean of at least three experiments. Additional statistical details are provided in the Supporting Information.

consistent with earlier accounts, k_{inact}/K_i proved to be a critical measure that differentiates these compounds (Table 1).^{18,19} Indeed, these data led to the selection of 2 and 3 for X-ray analysis, which subsequently led to the design of 4.

Cocrystal structures of PLP bound to hydroxamates 2 and 3 in the KAT II active site show intriguing changes to the protein. In the case of PLP adduct of compound 2 bound to KAT II, the overlay with a crystal structure of 1 bound to the same components highlights discrete differences (Figure 2), in particular with a domain consisting of Ile-19 to Gly-29, located at the entrance of the binding pocket.²⁰ In the structure containing hydroxamate 1, this domain is highly disordered. In contrast, the crystal structure containing 2 shows a highly ordered region.²¹ The 2-fold k_{inact}/K_i enhancement of derivative 2 as compared to parent may be attributed to an additional van der Waals interaction with Ile-19.

A previously unknown lipophilic interaction was discovered by introducing a phenoxy side chain at C-6. In the crystal structure containing compound 3 with KAT II, the aryl group rotates into a hydrophobic pocket found at the entrance to the active site and bounded on one face by Leu-293 (Figure 3), leading to a 1.5-fold boost in potency over compound 1 (Figure 3).²²

These unique interactions inspired the design of a disubstituted analogue that combined both key elements from compounds 2 and 3. To avoid the potential formation of a reactive metabolite characteristic of catechols, hydroxamate 4 was synthesized (Table 2). Interestingly, a 4–5-fold enhance-

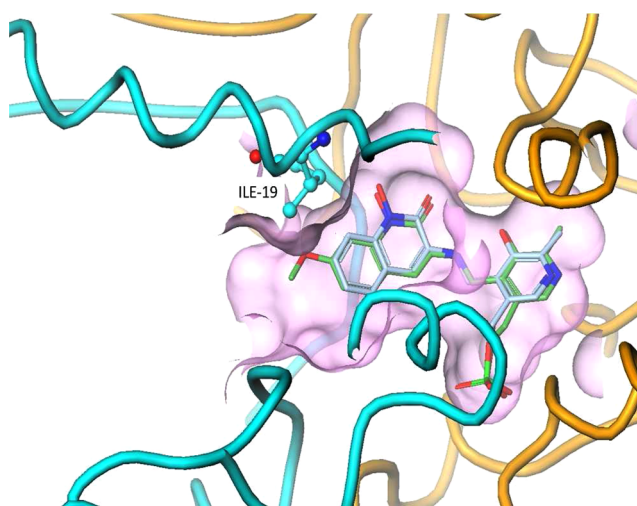


Figure 2. Superposition of the crystal structures of 1 and 2 with KAT II, showing the additional van der Waals interactions made by the methoxy substituent at C-7. The entire helix at the entrance of the binding pocket, consisting of residues Ile-19 to Gly-29, is disordered in the structure of PLP-bound 1 (yellow), whereas it is ordered in the structure of 2 (light blue).

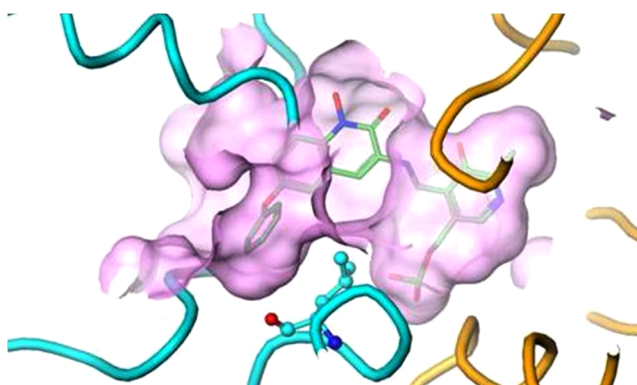


Figure 3. Crystal structure of 3 with KAT II. The C-6 phenoxy substituent of 3 orients into a shallow pocket at the mouth of the binding site, which is bounded on one face by Leu-293.

ment in potency was observed in the k_{inact}/K_i , an improvement not evidenced by the IC_{50} value of 4.

In the crystal structure of 4 bound to KAT II, in analogy to the structure of compound 3, the benzyl group is oriented into a lipophilic pocket framed by Leu-293.²³ Interestingly, an apparent cation– π interaction formed with Arg-20, the residue adjacent to Ile-19, and the phenyl ring (3.5 Å,²⁴ Figure 4). This type of interaction is well-known in proteins, where it plays a role in secondary and tertiary structure stabilization.^{25,26} The previously disordered region now acts as a clamp that anchors the hydroxamic acid–PLP complex into the active site and, as a result, enhances potency.²¹

It is intriguing to speculate that mechanistically, the 6-OMe may form lipophilic and/or hydrogen bond interactions with Ile-19 and Arg-20 on the α -helix that, upon orienting Arg-20 into a coplanar interaction with the benzyl group, is further stabilized by a hydrogen bond with the oxygen of the methoxy group. This bidentate interaction is only possible when both interactions are present, as this clamped architecture is not observed in the KAT II structures with 2 and 3 (Figure 5, compare to Figure 3). Additionally, this suggests that enthalpic

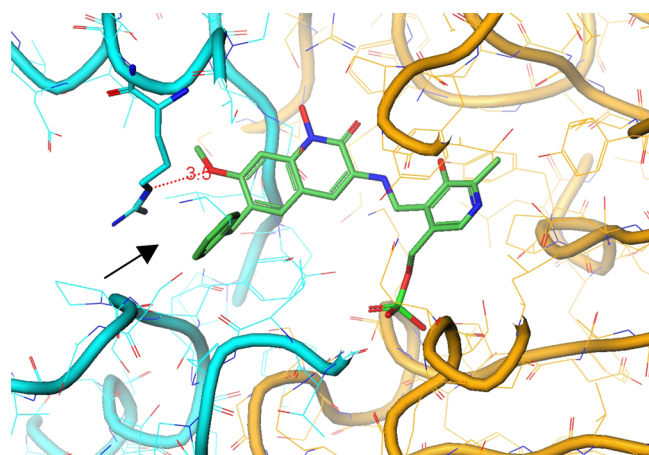


Figure 4. Crystal structure of 4 with KAT II. The combination of 7-OMe and 6-Bn substituents results in additional interactions with Arg-20. The arrow marks a potential cation- π interaction between the guanidium group in Arg-20 and the phenyl ring.

stabilization overrides the entropic loss and leads to this greatly improved potency.

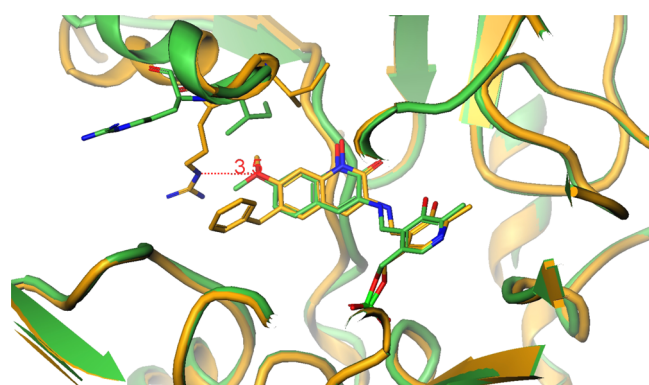


Figure 5. Overlay of crystal structures generated from 2 (green) and 4 (yellow). Two binding elements are necessary to interact with Arg-20.

Further analysis of the individual k_{inact} and K_i values provided insight into the nature of the enhanced potency. In the overall scheme of enzyme (E) inhibition by an irreversible inhibitor (I), the first step is reversible binding characterized by equilibrium binding dissociation constant K_i followed by the irreversible covalent bond forming event characterized by first-order inactivation rate constant k_{inact} (Scheme 1).²⁰

Scheme 1. Schematic of Irreversible Inhibition



For these analogues, k_{inact} values fall within a close range from 0.0108 to 0.0156 min^{-1} , indicating that the rates of covalent bond formation with PLP are similar. The difference lies in K_i , where there is a large discrepancy in values, indicating that the inhibition for these compounds is largely K_i driven (Tables 1 and 2, compare entries 1–4). In the event, analogue 4 binds to KAT II 5 \times more efficiently than 2 and 3.

Comparing entries 1 and 3 by in vivo microdialysis experiments illustrates the impact that increased potency has on lowering central KYNA. Subcutaneous administration of

each compound at 10 mg/kg results in a 9-fold lower free brain exposure of 3 as compared to 1 (65 ng h/g vs 584 ng h/g), due in part to the high nonspecific binding of 3 to brain tissue (Table 3, 99% bound). Nevertheless, compound 3 reduces

Table 3. PK of Compounds 1 and 3

| Compound | Structure | brain AUC ng ^h /g | free brain AUC (ng ^h /g) | Fu,b | rat k_{inact}/K_i ($\text{M}^{-1}\text{s}^{-1}$) ^c |
|----------|-----------|------------------------------|-------------------------------------|--------|--|
| 1 | | 1486 | 584 | 0.393 | 573 |
| 3 | | 6602 | 65 | 0.0099 | 9070 |

brain KYNA levels for a significantly longer period of time and to a greater degree than compound 1, at the same dose, as a result of its improved rat KAT II k_{inact}/K_i (Figure 6).

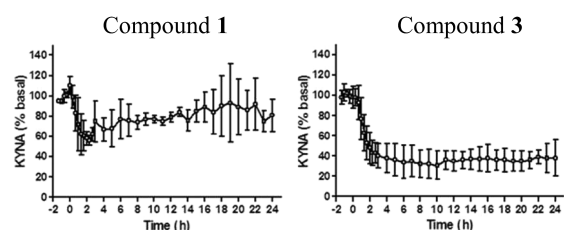


Figure 6. Prefrontal cortex extracellular levels of KYNA in freely moving rats measured using microdialysis. Compounds 1 and 3 were administered at 10 mg/kg sc at $t = 0$. Data are expressed as a percentage of preinjection baseline and are means \pm SEMs ($n = 4$).

The lowering of KYNA is attributed to the selective inhibition of KAT II as both compounds are weakly potent at KAT I and KAT III isoforms. Inhibitors 2 and 4 exhibited a similar selectivity profile.²⁷ While compound 4 was equipotent at rat KAT II ($k_{\text{inact}}/K_i = 763 \text{ M}^{-1} \text{ s}^{-1}$) as compared to compound 1, KYNA levels were not lowered at any dose due to high clearance. Currently, follow-up designs are focusing on lowering the clearance of compound 4, as the poor pharmacokinetics has a deleterious effect on in vivo efficacy.²⁸

In summary, X-ray crystallography and a k_{inact}/K_i assay led to the rational design of irreversible KAT II inhibitor 4. The crystal structure of this compound with KAT II led to the discovery of a novel interaction with a region previously found to be disordered. Ongoing efforts to optimize ligand interactions with the enzyme and improve pharmacokinetic properties will be reported in due course.

■ ASSOCIATED CONTENT

Supporting Information

Experimental data for the synthesis and characterization of compounds 3 and 4, assay protocols, and X-ray crystallography data. This material is available free of charge via the Internet at <http://pubs.acs.org>.

■ AUTHOR INFORMATION

Corresponding Author

*Tel: 617-395-0701. E-mail: jamison.b.tuttle@pfizer.com.

Present Address

[†]700 Main Street, Cambridge, Massachusetts 02139, United States.

Author Contributions

The manuscript was written through contributions of all authors. All authors have given approval to the final version of the manuscript.

Notes

The authors declare no competing financial interest.

ACKNOWLEDGMENTS

We thank Scot Mente and Ann Aulabaugh for helpful discussions. Katherine Brightly played a critical role in editing this manuscript. Zoe Hughes provided key insights into the analysis and depiction of the microdialysis data.

REFERENCES

- (1) Han, Q.; Cai, T.; Tagle, D. A.; Li, J. Structure, expression, and function of kynurenine aminotransferases in human and rodent brains. *J. Cell. Mol. Life Sci.* **2010**, *67*, 353–368.
- (2) Eliot, A. C.; Kirsch, J. F. Pyridoxal phosphate enzymes: Mechanistic, structural, and evolutionary considerations. *Annu. Rev. Biochem.* **2004**, *73*, 383–415.
- (3) Moroni, F.; Cozzi, A.; Sili, M.; Mannaioni, G. Kynurenic acid: A metabolite with multiple actions and multiple targets in brain and periphery. *J. Neural Transm.* **2012**, *119*, 133–139.
- (4) Hilmas, C.; Pereira, E. F.; Alkondon, M.; Rassoulpour, A.; Schwarcz, R.; Albuquerque, E. X. The brain metabolite kynurenic acid inhibits $\alpha 7$ nicotinic receptor activity and increases non- $\alpha 7$ nicotinic receptor expression: Physiopathological implications. *J. Neurosci.* **2001**, *21*, 7463.
- (5) Parsons, C. G.; Danysz, W.; Quack, G.; Hartmann, S.; Lorenz, B.; Wollenburg, C.; Baran, L.; Przegalinski, E.; Kostowski, W.; Krzascik, P.; Chizh, B.; Headley, P. M. Novel systemically-active antagonists of the glycine site of the NMDA receptor—Electrophysiological, biochemical and behavioural characterization. *J. Pharmacol. Exp. Ther.* **1998**, *283*, 1264–1275.
- (6) Erhardt, S.; Blennow, K.; Nordin, C.; Skogh, E.; Lindstrom, L. H.; Engberg, G. Kynurenic acid levels are elevated in the cerebrospinal fluid of patients with schizophrenia. *Neurosci. Lett.* **2001**, *313*, 96–98.
- (7) Nilsson, L. K.; Linderholm, K. R.; Engberg, G.; Paulson, L.; Blennow, K.; Lindstrom, L. H.; Nordin, C.; Karanti, A.; Persson, P.; Erhardt, S. Elevated levels of kynurenic acid in the cerebrospinal fluid of male patients with schizophrenia. *Schizophr. Res.* **2005**, *80*, 315–322.
- (8) Schwarcz, R.; Rassoulpour, A.; Wu, H.-Q.; Medoff, D.; Tamminga, C. A.; Roberts, R. C. Increased cortical kynurenate content in schizophrenia. *Biol. Psychiatry* **2001**, *50*, 521.
- (9) Olsson, S. K.; Samuelsson, M.; Saetre, P.; Lindstrom, L.; Jonsson, E. G.; Nordin, C.; Engberg, G.; Erhardt, S.; Landen, M. Elevated levels of kynurenic acid in the cerebrospinal fluid of patients with bipolar disorder. *J. Psychiatry Neurosci.* **2010**, *35*, 195–199.
- (10) Erhardt, S.; Olsson, S. K.; Engberg, G. Pharmacological manipulation of kynurenic acid: Potential in the treatment of psychiatric disorders. *CNS Drugs* **2009**, *23*, 91–101.
- (11) Potter, M. C.; Elmer, G. I.; Bergeron, R.; Albuquerque, E.; Guidetti, P.; Wu, H.-Q.; Schwarcz, R. Reduction of endogenous kynurenic acid formation enhances extracellular glutamate, hippocampal plasticity, and cognitive behavior. *Neuropsychopharmacology* **2010**, *35*, 1734–1742.
- (12) Schmidt, W.; Guidetti, P.; Okuno, E.; Schwarcz, R. Characterization of human brain kynurenine aminotransferases using [3H] kynurenine as a substrate. *Neuroscience* **1993**, *55*, 177–184.
- (13) Dounay, A. B.; Anderson, M.; Bechle, B. M.; Campbell, B. M.; Claffey, M. M.; Evdokimov, A.; Evrard, E.; Fonseca, K. R.; Gan, X.; Ghosh, S.; Hayward, M. M.; Horner, W.; Kim, J. Y.; McAllister, L. A.; Pandit, J.; Paradis, V.; Parikh, V. D.; Reese, M. R.; Rong, S.; Salafia, M. A.; Schuyten, K.; Strick, C. A.; Tuttle, J. B.; Valentine, J.; Wang, H.; Zawadzke, L. E.; Verhoest, P. R. Discovery of brain-penetrant, irreversible kynurenine aminotransferase II inhibitors for schizophrenia. *ACS Med. Chem. Lett.* **2012**, *3*, 187–192.
- (14) Claffey, M. M.; Dounay, A. B.; Gan, X.; Hayward, M. M.; Rong, S.; Tuttle, J. B.; Verhoest, P. R. Bicyclic and Tricyclic Compounds as KAT II inhibitors. WO2010146488.
- (15) Pellicciari, R.; Rizzo, R. C.; Costantino, G.; Marinozzi, M.; Amori, L.; Guidetti, P.; Wu, H.-Q.; Schwarcz, R. Modulators of the kynurenine pathway of tryptophan metabolism: synthesis and preliminary biological evaluation of (S)-4-(ethylsulfonyl)-benzoylalanine, a potent and selective kynurenine aminotransferase II (KAT II) inhibitor. *ChemMedChem* **2006**, *1*, 528–531.
- (16) Schwarcz, R.; Kajii, Y.; Ono, S. Preparation of aminopiperazinyloquinolonecarboxylates as kynurenine-aminotransferase inhibitors. WO2009064836.
- (17) In the event, when measuring KYNA in dialysates from rat prefrontal cortex, a 10 mg/kg dose, sc, showed a 50% decrease from basal levels that returned to baseline approximately 20 h postdose.
- (18) Mileni, M.; Johnson, D. S.; Wang, Z.; Everdeen, D. S.; Liimatta, M.; Pabst, B.; Bhattacharya, K.; Nugent, R. A.; Kamtekar, S.; Cravatt, B. F.; Ahn, K.; Stevens, R. C. Structure-guided inhibitor design for human FAAH by interspecies active site conversion. *Proc. Natl. Acad. Sci. U.S.A.* **2008**, *105*, 12820–12824.
- (19) Copeland, R. A. *Evaluation of Enzyme Inhibitors in Drug Discovery: A Guide for Medicinal Chemists and Pharmacologists*; Wiley: Hoboken, NJ, 2005; pp 1–265.
- (20) The coordinates have been deposited in the Protein Data Bank, with ID 4GE4.
- (21) Average B values (in Å^2) for Arg-20 in each of the structures are as follows: 1 = no value, too disordered; 2 = 84.90; 3 = 103.35; and 4 = 27.30
- (22) The coordinates have been deposited in the Protein Data Bank, with ID 4GE7.
- (23) The coordinates have been deposited in the Protein Data Bank, with ID 4GE9.
- (24) See the Supporting Information for the distance measurement method and corresponding figure.
- (25) Gallivan, J. P.; Dougherty, D. A. Cation- π interactions in structural biology. *Proc. Natl. Acad. Sci. U.S.A.* **1999**, *96*, 9459–9464.
- (26) Crowley, P. B.; Golovin, A. Cation- π interactions in protein-protein interfaces. *Proteins: Struct., Funct., Bioinf.* **2005**, *59*, 231–239.
- (27) Compound 1: hKAT I IC_{50} = 30.4 μM and hKAT III IC_{50} = 9.04 μM . Compound 2: hKAT II IC_{50} = 15.3 μM and hKAT II IC_{50} = 6.4 μM ; for comparison purposes, rat KAT II k_{inact}/K_i = 1840 $\text{M}^{-1} \text{s}^{-1}$. Compound 3: hKAT I IC_{50} = 2.04 μM and hKAT III IC_{50} = 1.23 μM . Compound 4: hKAT I IC_{50} > 36 μM and hKAT III IC_{50} = 13.6 μM .
- (28) Dosing compound 4 in male rats at 32 mg/kg sc had no lowering effect on PFC kynurenic acid levels as measured by microdialysis.